Journal of Colloid and Interface Science 624 (2022) 546–554

Contents lists available at ScienceDirect

Journal of Colloid and Interface Science

journal homepage: www.elsevier.com/locate/jcis

Microfluidic electrospray generation of porous magnetic Janus reduced graphene oxide/carbon composite microspheres for versatile adsorption

Xiaomin Ye [a,b], Yunru Yu [c], Chaoyu Yang [c], Qihui Fan [a,*], Luoran Shang [d,*], Fangfu Ye [a,b,c,e,*]

[a] Beijing National Laboratory for Condensed Matter Physics, Institute of Physics, Chinese Academy of Sciences, Beijing 100190, China
[b] School of Physical Sciences, University of Chinese Academy of Sciences, Beijing 100049, China
[c] Wenzhou Institute, University of Chinese Academy of Sciences, Wenzhou, Zhejiang 325001, China
[d] Shanghai Xuhui Central Hospital, Zhongshan-Xuhui Hospital, and the Shanghai Key Laboratory of Medical Epigenetics, the International Co-laboratory of Medical Epigenetics and Metabolism (Ministry of Science and Technology), Institutes of Biomedical Sciences, Fudan University, Shanghai 200032, China
[e] Oujiang Laboratory (Zhejiang Lab for Regenerative Medicine, Vision and Brain Health), Wenzhou, Zhejiang 325001, China

GRAPHICAL ABSTRACT

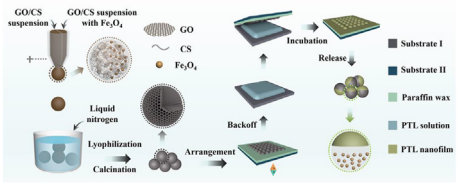

ARTICLE INFO

Article history:
Received 22 April 2022
Revised 22 May 2022
Accepted 28 May 2022
Available online 1 June 2022

Keywords:
Microfluidic electrospray
rGO/C composites
Janus magnetic particle
Surface wettability
Versatile adsorption

ABSTRACT

Hypothesis: Graphene-based microparticles materials are broadly utilized in all sorts of fields owing to their outstanding properties. Despite great progress, the present graphene microparticles still face challenges in the aspects of size uniformity, motion flexibility, and tailorable surface chemistry, which limit their application in some specific fields, such as versatile adsorption. Hence, the development of novel graphene microparticles with the aforementioned characteristics is urgently required.
Experiments: We presented a simple microfluidic electrospray strategy to generate magnetic Janus reduced graphene oxide/carbon (rGO/C) composite microspheres with a variety of unique features. Specifically, the microfluidic electrospray method endowed the obtaiend microspheres with sufficient size uniformity as well as magnetic responsive motion ability. Additionally, magnetic-mediated surface assembly of phase transition lysozyme (PTL) nanofilm on the microspheres rendered the deposited area hydrophilic while non-deposited area hydrophobic.
Findings: Such magnetic Janus rGO/C composite microspheres with regionalized wettability characteristics not only showed prominent performance in adsorbing organic liquids with high adsorption capacity and remarkable reusability but also displayed satisfying biocompatibility for the efficient uptake of bilirubin. More encouragingly, the microspheres could serve as adsorbents in a simulative hemoperfusion setup, which further demonstrated the clinical application potential of the magnetic Janus rGO/C microspheres. Thus, we anticipate that the obtained magnetic Janus rGO/C composite microspheres could show multifunctional properties toward water treatment and blood molecule cleaning.

1. Introduction

Graphene has attracted considerable attention owing to its intriguing features such as high specific surface area, excellent

* Corresponding authors.
E-mail addresses: fanqh@iphy.ac.cn (Q. Fan), luoranshang@fudan.edu.cn (L. Shang), fye@iphy.ac.cn (F. Ye).

https://doi.org/10.1016/j.jcis.2022.05.156
0021-9797/

electrical conductivity, ultralightweight, and so on [1–3]. Over the past decades, graphene has been processed into various materials including 3D bulk spongy graphene, graphene-polymer composite film, porous graphene foam, etc [4–7]. These materials are extensively utilized in environmental protection, electrochemical energy devices, supercapacitors, sensors, to list a few [8–10]. In particular, many efforts have been focused on developing graphene-based microparticles [11,12]. Microparticles have the large surface area and are flexible to manipulate, thereby demonstrating superiorities over traditional bulk materials [13,14]. Specifically, graphene-based microparticles owned hybrid compositions and hierarchical porous structure, thus showing greater potential towards multiple application areas such as water decontamination, enrichment of glycopeptide, blood purification, etc [15–17]. For intance, Cheng et al. developed utralight NiCo@reduced graphene oxide (NiCo@rGO) aerogel microspheres with highly hierarchical porous structure and hydrophobic feature through electrospray approach [18]. The resultant NiCo@rGO aerogel microspheres exhibited extraordinary oil/water separation efficacy with maximum uptake capacities of 270 g/g. In another attempt, Luo et al. reported photothermal carbon nanotube/reduced graphene oxide (CNT/rGO) aerogel microspheres with radial inner microchannels aiming at efficient cleaning of crude oil [19]. Apart from this, Wu et al. fabricated nanoporous chitosan/graphene oxide (CS/GO) composite microspheres with excellent bilirubin remvol performance [20]. Despite these progress, these microspheres still face the dilemma of polydispersity, unsatisfactory separation and recovery, or limited application scenarios. Hence, the development of graphene microparticles with combinatorial properties of uniform size, controllable motion, and tailorable surface chemistry is highly desired.

In this paper, we employed a facile microfluidic electrospray strategy for the fabrication of Janus graphene composite microspheres with integrated properties of size uniformity, magnetic-induced motion ability, as well as tailored surface wettability, as schemed in Fig. 1. Owing to its remarkable controllability of the shape, structure, and components of the final products, microfluidic technology is the superior method for microparticles production, such as microgels, colloidal crystal beads, etc., in the form of simple microspheres, Janus/multicompartmental spheres, microcapsules, and non-spherical particles [21–32]. However, for the fabrication of graphene-based particles, the majority of the existing microfluidic platforms adopt a simple emulsion system, which does not essentially improve the functions of the resultant particles.

Herein, we utilized a double-channel microfluidic setup to prepare magnetic Janus reduced graphene oxide/carbon (rGO/C) composite microspheres. The obtained microspheres possessed a variety of unique features. On one hand, the microfluidic electrospray strategy imparted the final particles with sufficient size uniformity, which was pivotal to the performance stability (Fig. 1**a**). On the other hand, by adding magnetic nanoparticles (NPs) to one of the flow channels, one hemisphere of the Janus particles could respond to the magnetic field, thereby enabling controllable movement of the resultant microspheres. Besides, versatile assembly of phase transition lysozyme (PTL) nanofilm on the particle surface was achieved, rendering the deposited area hydrophilic while non-deposited area hydrophobic (Fig. 1**b**). Such regionalized wettability characteristics made the composite microspheres applicable to more scenarios including in the uptake of water pollutants and removal of excess bilirubin. These performances indicated that the present magnetic Janus rGO/C composite microspheres are excellent materials for versatile adsorption and could find great value in environmental protection and hyperbilirubinemia therapy.

2. Results and discussion

2.1. Generation of the magnetic Janus rGO/C composite microspheres

In a typical experiment, the preparation of the magnetic Janus rGO/C composite microspheres included three key steps, namely microfluidic electrospray, lyophilization, and high-temperature carbonization. A microfluidic device with a θ-shaped fluid outlet was constructed to induce an acetic acid suspension of GO/chitosan (CS) and a Fe_3O_4 NPs-doped GO/CS acetic acid suspension separately for electrospray (Fig. 1**a**). With a sufficient voltage, the charged suspensions could split into a stream of droplets. The droplets fell into a container filled with liquid nitrogen and formed Janus GO/CS ice balls instantly. Subsequently, the ice balls underwent lyophilization by which their internal structure was maintained. Further, high-temperature carbonization treatment was carried out and Janus reduced graphene oxide (rGO)/C microspheres with uniform size were eventually acquired (Fig. 2**a**). It was worth noting that owing to the similar dark color of GO and magnetic NPs and the easy melting feature of the ice balls, it was difficult to distinguish the Janus structure. Hence, we prepared microspheres with one half of pure CS and the other half of magnetic NPs-doped CS to enhance the color contrast. Besides, we solidified the microspheres by immersing them to a sodium hydroxide solution. With that, we were able to examine the Janus construction of the resultant microspheres (Fig. 2**b**). Due to the anisotropic arrangement of the magnetic NPs, the Janus

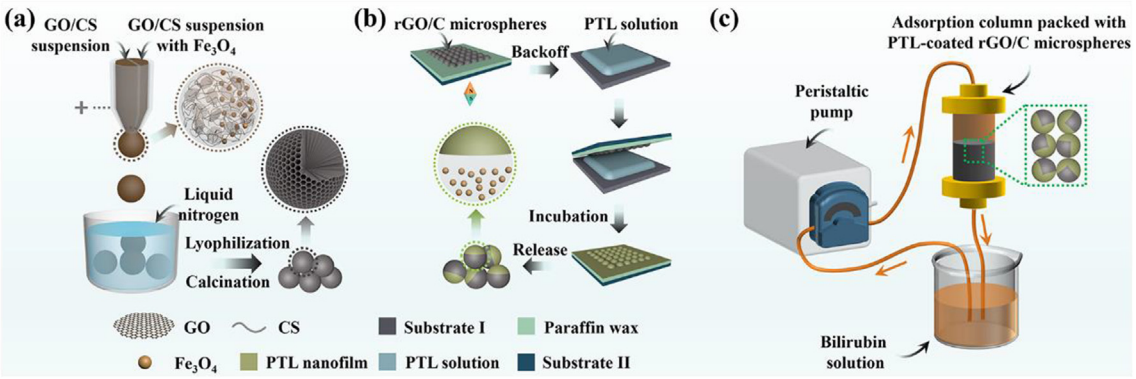

Fig. 1. (a) Sketch map of the generation process of the magnetic Janus rGO/C composite microspheres. Note: the positive terminal of the DC power supply was connected to the stainless steel needles of the syringes containing GO/CS dispersions, and the negative terminal was grounded; (b) sketch map of the surface self-assembly of the PTL nanofilm on the magnetic Janus rGO/C composite microspheres mediated by a permanent magnet; (c) sketch map of the process of a simulative bilirubin-removal apparatus with PTL-coated magnetic Janus rGO/C microspheres as the sorbents according to the present clinical hemoperfusion technology.

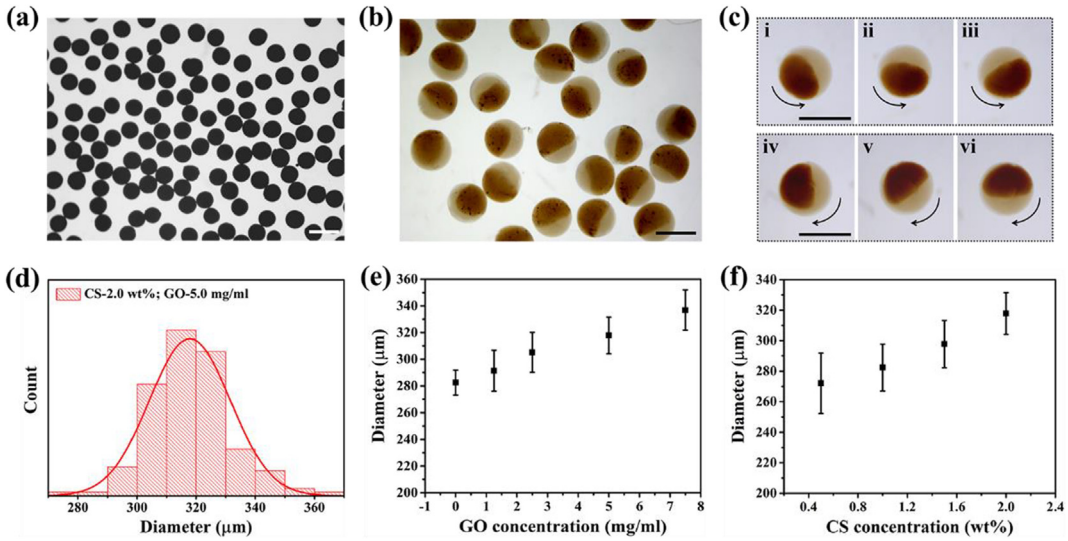

Fig. 2. (a) Optical image of the magnetic Janus $rGO_{5.0}$/C microspheres after carbonization; (b) optical image of the magnetic Janus microspheres with one half of pure CS and the other half of magnetic NPs-doped CS; (c) magnetic-induced motion of the Janus microspheres, which showed clockwise or anticlockwise rotation, depending on the magnetic field; (d) the size distribution of the magnetic Janus $rGO_{5.0}$/C microspheres; (e) the diameter of the magnetic Janus rGO/C microspheres as a function of the GO content in the precursor suspension; (f) relationship between the diameter of the magnetic Janus rGO/C microspheres and CS content in precursor suspension. Scale bars are 500 μm in (a-c).

microspheres could rotate in the direction of an attached magnet, as shown in Fig. 2**c**.

Notably, random interaction of rGO nanosheets usually leads to a fragile and irregular structure [33]. Here, we introduced CS as a binder to improve the mechanical strength of the microspheres. Chitosan, as a type of renewable resource, is cost-effective and is comprised of abundant reactive groups such as amine and hydroxyl groups. Positively charged CS can attach to negatively charged GO nanosheets through electrostatic interaction, resulting in a GO-based 3D network architecture with remarkable stability [33]. Taking advantage of this, we acquired porous magnetic Janus rGO/C composite microspheres with robust and regular structures (Fig. 2**a**). In addition, we investigated the influence of the GO and CS content on the size of the magnetic Janus rGO/C composite microspheres. It was observed that the diameter of the microspheres both increased with the GO content or CS content (Fig. 2**-d-2f**). The above result could be ascribed to the increased overall viscosity of the GO/CS precursor suspension with the increase of either GO or CS content. It was worth mentioning that when the concentration of CS was lower than 2.0 wt%, the obtained composite microspheres were still fragile. Therefore, we chose 2.0 wt% for the fabrication of rGO/C composite microspheres in the following experiments.

2.2. Characterization of the magnetic Janus rGO/C composite microspheres

The scanning electron microscope (SEM) was employed to observe the morphology and microstructure of the magnetic Janus rGO/C composite microspheres. During the fabrication process, the ice crystals in the ice ball grew along the radial direction. Subsequently, after lyophilization, the ice crystals were removed, leaving a radially oriented microchannel structure [34]. Therefore, it could be observed that the magnetic Janus rGO/C composite microspheres exhibited a spherical morphology accompanied by porous honeycomb-like structures at the surface (Fig. 3**a and 3d**). Meanwhile, we cut a microsphere to observe the cross-section structure, which exhibited a radially oriented channel construction (Fig. 3**b and 3e**). Besides, the enlarged images showed that the width of the internal microchannels was at the micron scale (Fig. 3**c and 3f**). Furthermore, the Brunauer Emmertt Teller (BET) specific surface area results in **Table S1** showed that the value slowly increased with the GO content in the precursor suspension. Such interior microchannel architecture and high specific surface area could facilitate diffusion, thereby dramatically improving the adsorption capacity.

To evaluate the phase structure and chemical component of the rGO/C composite samples, a series of analytical approaches were carried out. To begin with, the x-ray diffraction (XRD) pattern of $rGO_{5.0}$/C composite in Fig. 4**a** displayed a sharp characteristic peak of 10.5°. This is designated as the (002) crystallographic plane of GO [35]. Besides, a wide diffraction peak located at 19.9°, which was nominated as the (110) plane of CS [36]. After carbonization, the characteristic peaks of CS and GO did not exist in the sample while a new wide peak around 26° appeared. Hence, it could be concluded that the GO/CS composite has been successfully transformed to graphitic carbon after carbonization [36–38]. Besides, when GO content increased, the XRD characteristic peak of the $rGO_{5.0}$/C composite gradually approached from from CS-C to rGO, implying the decrease of amorphous carbon and increase of ordered carbon (**Fig. S1a**). However, when the GO content was fixed at 5 mg/ mL or above, the diffraction peak of graphitic carbon remained in the same position regardless of the CS content in the precursor suspension (**Fig. S1b**), indicating that the crystal structure of graphitic carbon was dominated by rGO. Moreover, the Fourier transform infrared spectroscopy (FTIR) was used to further identify the molecular structure of the rGO/C composite. Fig. 4**b** displayed a variety of characteristic peaks because of abundant functional groups of GO and CS. Interestingly, it was found that the FTIR curve of the rGO/C composite became quite smooth after calcination, again suggesting that the rGO/C sample possessed a high degree of graphitization [35,39].

We also analyze the chemical composition of the obtained rGO/C sample through x-ray photoelectron spectroscopy (XPS) spectra. Fig. 4**c** verified the presence of the elements O, N, and C in the rGO/C sample. Notably, compared to CS, the intensity of element O dramatically reduced because of the removal of most oxygen functional groups after carbonization. As a result, the amount

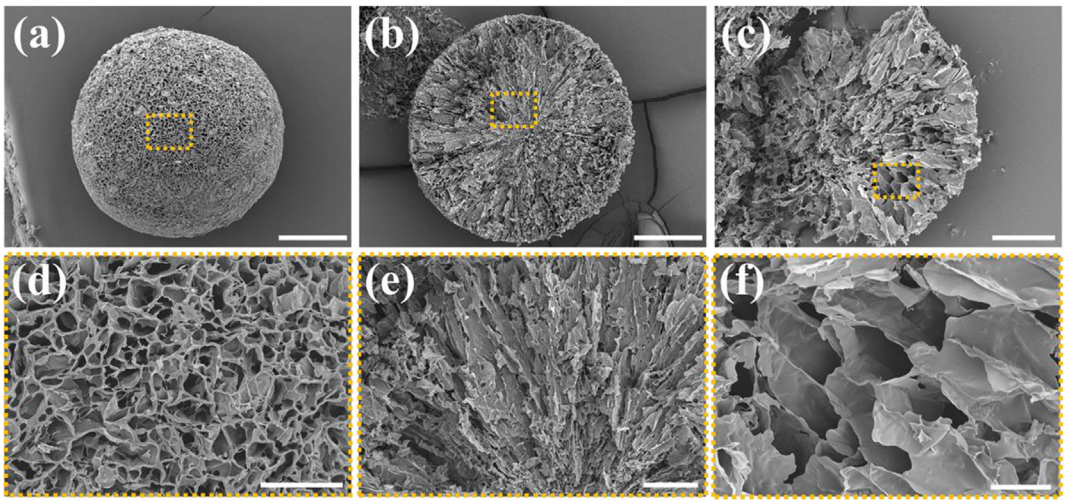

Fig. 3. SEM images of the magnetic Janus rGO/C composite microspheres: (a) an intact magnetic Janus $rGO_{5.0}$/C microsphere (scale bar, 100 μm); (b, c) the cross-section of a magnetic Janus $rGO_{5.0}$/C microsphere ((b), scale bar, 100 μm; (c), scale bar, 50 μm); (d-f) the enlarged view of (a-c), respectively ((d) and (e), scale bar, 20 μm; (f), scale bar, 10 μm).

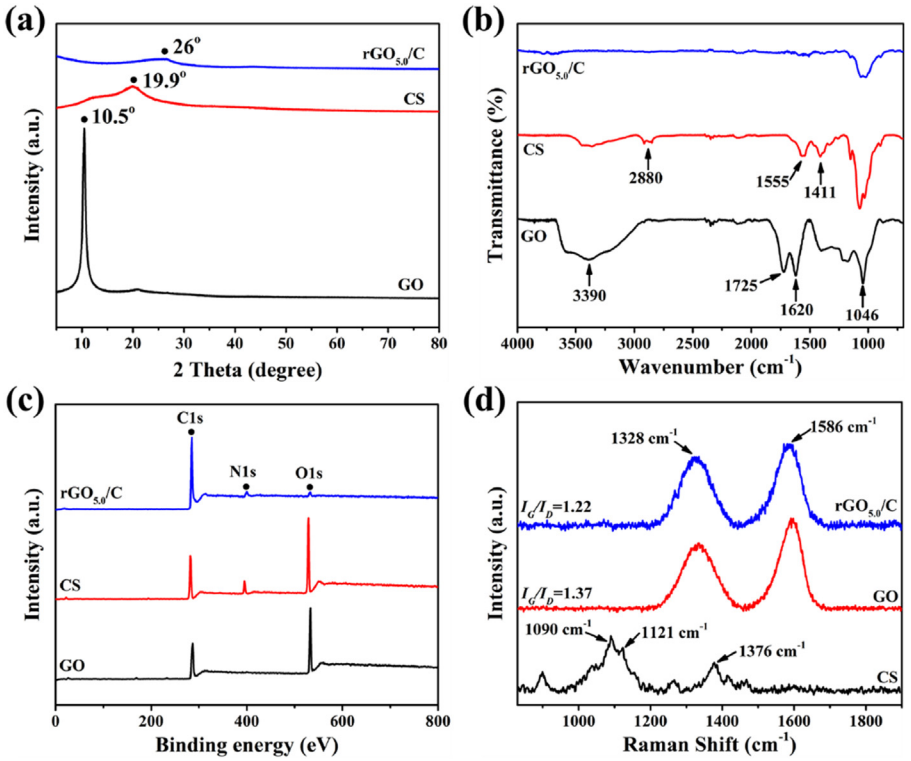

Fig. 4. (a) XRD patterns of GO, $rGO_{5.0}$/C, and CS; (b) FTIR spectra of GO, $rGO_{5.0}$/C, and CS. For GO, the adsorption peaks of 1046 cm^{-1}, 1620 cm^{-1}, and 1725 cm^{-1}, 3390 cm^{-1} were correlated with the epoxy group, the aromatic ring, the carbonyl group, and hydroxyl group respectively; For CS, the adsorption peaks of 1411 cm^{-1}, 1555 cm-1, and 2880 cm^{-1} indicated C—N stretching vibration, the –NH bending of NH_2, and the C—H stretching vibration, respectively. (c) XPS spectra of GO, CS, and $rGO_{5.0}$/C; (d) Raman spectra of CS, GO, and $rGO_{5.0}$/C. For GO and $rGO_{5.0}$/C, 1586 $cm^{-1}$and 1328 cm^{-1} were designated as the G-band and D-band, respectively; for CS, 1090 cm^{-1} and 1121 cm^{-1} were derived from the symmetric vibrations of glycosidic bonds;1376 cm^{-1} was associated with CS backbone.

of element C significantly increased in comparison with that of GO or CS. Additionally, the high-resolution C_{1s} spectra and N_{1s} spectra in **Fig. S1c, S1d** reflected three characteristic peaks, namely, pyridinic N (398.5 eV), pyrrolic N (400.5 eV), and graphitic N (402.2 eV). The above peaks implied that the rGO/C composite has been converted to *N*-doped carbon [35,36]. Last but not least, Raman spectra were plotted in Fig. 4**d**. Two typical peaks located at 1586 $cm^{-1}$and 1328 cm^{-1} were defined as G-band and D-band. The G-band represents the vibrational modes of the sp^2-bonded carbon atoms in graphitic layer, whereas the D-band is associated with the defects in the graphene lattice [40]. The corresponding intensity ratio I_G/I_D is widely utilized to estimate the graphitization degree in the carbon materials. It could be observed that the I_G/I_D value of rGO/C sample (1.22) was slightly less than that of GO sample (1.37), which could be ascribed to a decrease in the average size of the sp^2 domains. Thus, the present rGO/C sample owned a

remarkable graphitization degree, which was in agreement with that of XRD and FITR.

2.3. Assembly of PTL nanofilm on magnetic Janus rGO/C composite microspheres

Since the magnetic Janus rGO/C composite microspheres consisted of rGO and carbonized chitosan, they were intrinsically hydrophobic. To endow the microspheres with tailorable wettability properties, surface self-assembly of PTL nanofilm was performed on the microspheres. PTL, an amyloid-like protein, could readily bind with virtually arbitrary substrates and plentiful hydrophilic groups of PTL could impart the substrate with the hydrophilic feature [41–44]. In addition, benefiting from the magnetic Janus structure, the rGO/C composite microspheres could rotate so that part of their surface could be deposited with a PTL nanofilm layer. With that, we could create microspheres with controllable coated areas by repeating the assembly process with the aid of a rotary magnetic field (Fig. 1**b and 5a**). We confirmed this through SEM imaging of the microspheres. As shown in Fig. 5**bi-5biii**, after multiple times of PTL nanofilm assembly, the coated area, manifested as a smooth and dense membrane (Fig. 5**biv-5bvi**), was gradually enlarged on the surface of the original porous microspheres. Furthermore, we confirmed the amyloid-like constituent in PTL nanofilm via Thioflavin T (ThT) staining. ThT is a benzothiazole dye that presents enhanced fluorescence when combined with amyloid fibrils [41]. Accordingly, the coated region could show fluorescence under a confocal laser scanning microscope (CLSM). It also could be found that the area of the fluorescent region expanded with the times of PTL nanofilm coating (Fig. 5**c**).

2.4. Adsorption of organic liquids using magnetic Janus rGO/C microspheres

Since PTL nanofilm has been successfully assembled at the surface of the magnetic Janus rGO/C microspheres, the region covered by PTL nanofilm should be rendered hydrophilic while the undeposited area should remain hydrophobic. We confirmed this from contact angle measurement. As expected, a water droplet placed on an original magnetic Janus rGO/C membrane could stay for a long time without any change and the contact angle measurement manifested a high water contact angle value (WCA) of 150° (Fig. 6**a**). By contrast, an oil droplet rapidly penetrated the membrane and the oil contact angle (OCA) was 0° (**Fig. S2**). After PTL

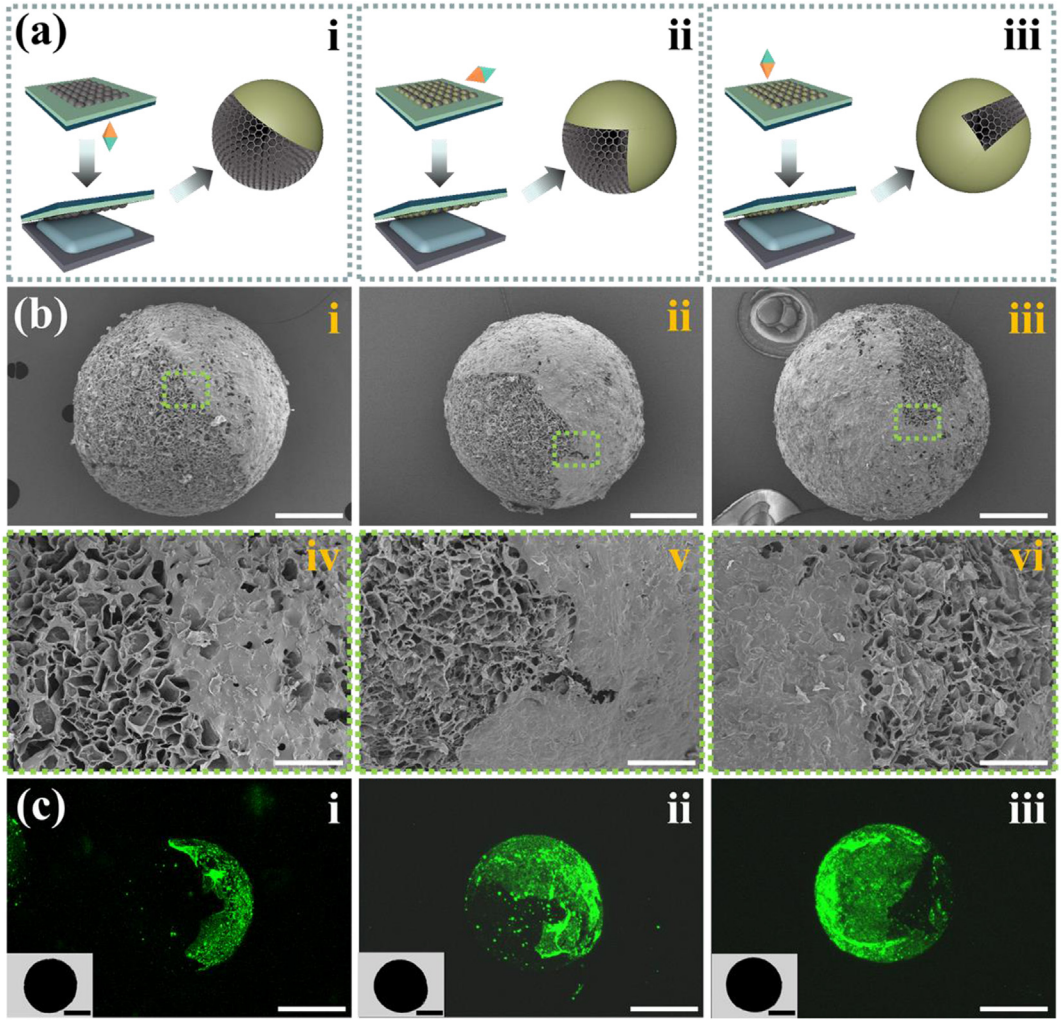

Fig. 5. (a) Sketch map of the surface self-assembly of PTL nanofilm on the microspheres mediated by a magnetic field; (b) SEM images of PTL coated- magnetic Janus rGO/C composite microspheres. i, ii, and iii represented 1, 2, and 3 times of PTL assembly, respectively. (iv-vi) are magnified images corresponding to (i-iii), which show the boundaries between coated and uncoated areas; Scale bars are 100 μm in (i-iii), and 25 μm in (iv-vi). (c) CLSM images of the magnetic Janus rGO/C microspheres after (i) 1, (ii) 2, and (iii) 3 times of PTL nanofilm assembly. PTL was stained with ThT, presenting enhanced fluorescence intensity. Inserted images are the corresponding bright-field view of the microspheres after PTL coating. Scale bar is 150 μm.

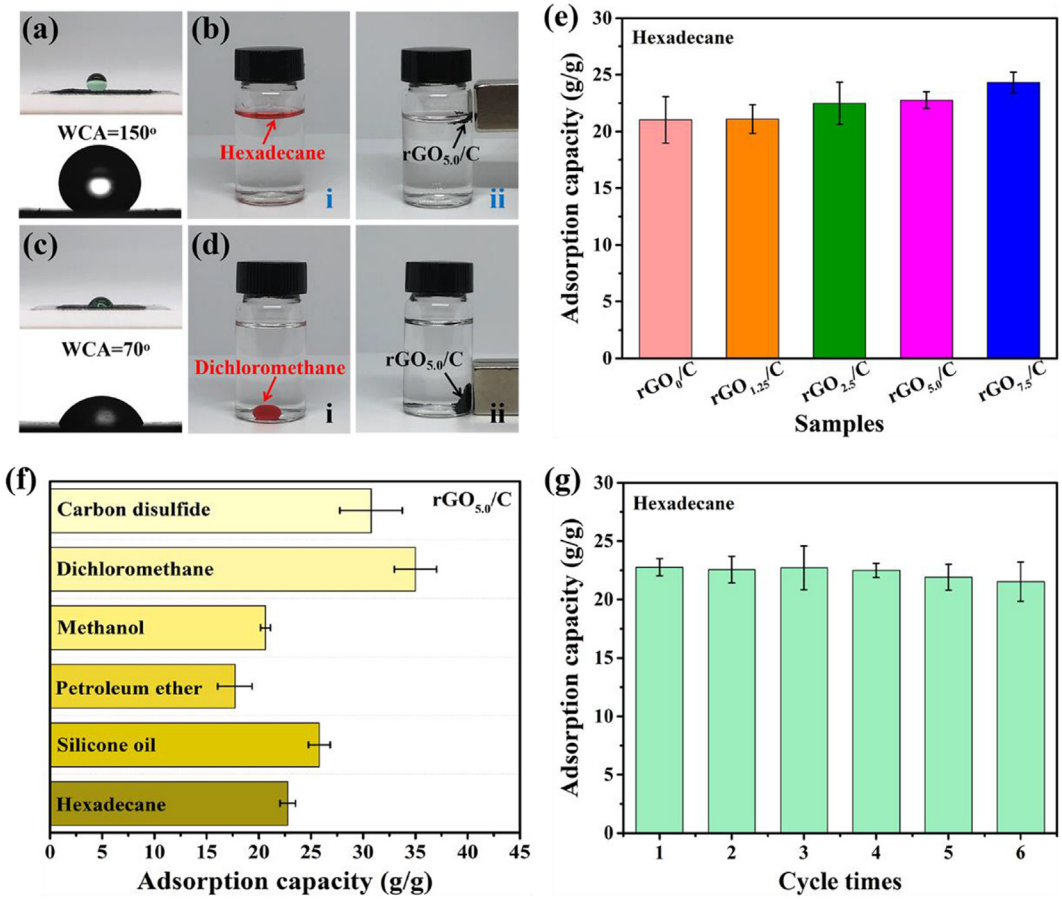

Fig. 6. (a) WCA of an initial rGO/C membrane; (b) photographs showing the adsorption of hexadecane by the magnetic Janus rGO/C microspheres; (c) WCA of a rGO/C membrane covered with a PTL nanofilm; (d) pictures displaying the uptake of dichloromethane by the PTL-coated magnetic Janus rGO/C microspheres; (e) uptake capacity of the magnetic Janus rGO/C microspheres with distinct rGO content toward hexadecane; (f) uptake capacity of the magnetic Janus $rGO_{5.0}$/C microspheres toward different organic liquids; (g) recyclability test of the magnetic Janus $rGO_{5.0}$/C microspheres for adsorbing hexadecane. All the tests were repeated 3 times.

nanofilm assembly, the WCA of the membrane changed to 70°, indicating the hydrophilic feature (Fig. 6**c**). These results manifested that the intrinsic hydrophobic and oleophilic magnetic Janus rGO/C composite microspheres could turn hydrophilic by PTL coating. Thus, the magnetic Janus rGO/C microspheres could be applied to the adsorption of organic liquids both floating on water and underwater. To demonstrate this, the uncoated magnetic Janus rGO/C microspheres were first employed to adsorb organic solvent floating on water due to their hydrophobicity and low density. As shown in Fig. 6**bi**, the red-dyed hexadecane disappeared quickly after casting magnetic Janus rGO/C microspheres, indicating the efficient adsorption. As for contaminants underwater, the PTL-coated magnetic Janus rGO/C microspheres were applied benefiting from their regionalized hydrophilicity. As shown in Fig. 6**di**, the red-dyed dichloromethane could be rapidly adsorbed by the PTL-coated magnetic Janus rGO/C microspheres. These results demonstrated the versatile adsorption ability of the magnetic Janus rGO/C microspheres. More intriguingly, both the uncoated and coated microspheres could achieve convenient collection by using a magnet (Fig. 6**bii and 6dii**), thereby realizing the collection of the adsorbate and the recovery of the sorbents.

To investigate the influence of the rGO content on the uptake efficiency, the magnetic Janus rGO/C microspheres with distinct rGO contents were applied in the removal of hexadecane. It was observed that the uptake capacity enlarged slightly with the rGO content (Fig. 6**e**). An increase in the specific surface area might account for this phenomenon. Additionally, to explore the uptake capacity of the magnetic Janus rGO/C microspheres for different contaminants, six types of pollutants, including hexadecane, silicone oil, petroleum ether, methanol, dichloromethane, and carbon disulfide, were chosen as the target adsorbates. It was found that the magnetic Janus $rGO_{5.0}$/C microspheres showed prominent performance in removing these pollutants with a maximum uptake capacity of 18–35 times of their weight (Fig. 6**f**). Such high adsorption capacity could be attributed to both strong affinities between adsorbates and adsorbents and the porous surfaces and radial internal microchannels, which facilitated the diffusion of the adsorbates. It was worth mentioning that, the adsorption capacity varied among different pollutants, which might be ascribed to the differences of their properties including density, viscosity, polarity, and so on [40]. Moreover, we tested the reusability of the microspheres by taking hexadecane as an example and measured the adsorption capacity for six cycles. As illustrated in Fig. 6**g**, the magnetic Janus $rGO_{5.0}$/C microspheres could retain 94.5% of their maximum adsorption capacity through 6 cycles, indicating the practical value for efficient adsorption of organic liquids.

2.5. Bilirubin adsorption using PTL-coated magnetic Janus rGO/C microspheres

To further prove the versatile adsorption property of the rGO/C microspheres, we conducted adsorption experiments for bilirubin. Bilirubin is a lipophilic pathogenic toxin derived from hemoglobin metabolism and the excess bilirubin can cause severe damage to

human health [45]. Thus, the elimination of excess bilirubin is vital to patients since they would obtain enough time to recover without worrying about the terrible influence caused by hyperbilirubinemia. Practically, hemoperfusion has been considered as a promising method for removing bilirubin, which relied on sorbents filled in a perfusion apparatus [46,47]. As such, the sorbents should possess high removal ability and considerable blood compatibility. Therefore, we investigated these properties of the PTL-coated magnetic Janus rGO/C microspheres. We first plotted the adsorption dynamics of rGO_0/C, $rGO_{1.25}$/C, $rGO_{2.5}$/C, $rGO_{5.0}$/C, and $rGO_{7.5}$/C microspheres toward bilirubin (see SI for the specific calculation process). As illustrated in Fig. 7**a**, the uptake capacity exhibited a rapid increase in the first 20 min, reaching about 50% of the maximum adsorption capacity. Afterwards, the dynamic curve rose gently until reaching equilibrium (Fig. 7**a**). Besides, a pseudo-second-order model was adopted to analyze the kinetics data, and the fitting results were shown in **Fig. S2b and Table S2 (**see SI for the specific fitting process). Apparently, with the increase of the GO content in precursor suspension, the removal capacity significantly improved, indicating that rGO could promote bilirubin adsorption. On one hand, the honeycomb-like porous surface and the radially oriented microchannels facilitated the uptake of bilirubin [33]. On the other hand, the π-π interactions among rGO nanosheets and tetrapyrrole rings of bilirubin effectively enhanced the adhesion of microspheres towards bilirubin [16,48]. It was worth mentioning that higher GO addition in the precursor suspension would pose difficulty in electrospray due to the increased viscosity of the suspension. Hence, the highest amount of GO in the precursor suspension was 7.5 mg/ml.

Next, we investigated the adsorption isotherms of the PTL-coated magnetic Janus $rGO_{5.0}$/C microspheres. It was observed that the uptake capacity of the microspheres increased dramatically with the initial bilirubin concentration and then slowly when the concentration exceeded 300 mg/L (Fig. 7**b**). Besides, we adopted Freundlich and Langmuir models to fit the isotherm data, the former of which is suited for the multilayer uptake process, while the latter is often applied to the monolayer uptake process [49]. The fitting curves were plotted in **Fig. S3b and 3c,** and the corresponding parameters were summarized in **Table S3.** Obviously, the Langmuir model fitted better than the Freundlich model, demonstrating a monolayer-dominated bilirubin adsorption process(see SI for the specific fitting process).

Based on these results, we further explored the practical application ability of the PTL-coated magnetic Janus rGO/C microspheres in clinical hemoperfusion. Specifically, to simulate real hemoperfusion equipment, we constructed a perfusion apparatus consisting of an adsorption column, a peristaltic pump, and a silicone tube (Fig. 1**c and 7c**). The adsorption column was filled with the PTL-coated magnetic Janus rGO/C microspheres as absorbents, and a continuous stream of bilirubin solution flowed through the column. Then, dynamic adsorption tests were conducted. As shown in Fig. 7**d**, compared with the magnetic Janus rGO_0/C microspheres, the magnetic Janus $rGO_{5.0}$/C microspheres had a faster removal rate and higher uptake capacity, due to abundant π π interactions between the magnetic Janus $rGO_{5.0}$/C microspheres and bilirubin. Besides, we examined the influence of flux on uptake efficiency. By increasing the flux from 1 ml/min to 2.5 ml/min, the microspheres exhibited an evident decrease in the adsorption capacity (**Fig. S3d**). We speculated that a higher flow rate could cause inadequate contact between bilirubin and the sorbents, which may account for the lower uptake capacity.

Since hemoperfusion sorbents have direct contact with human blood, their blood compatibility is a prerequisite. To verify this property, we first conducted an *in vitro* hemolysis assay by measuring the amount of hemoglobin in the supernatant. Notably, PBS buffer and deionized water were served as the negative and positive control. As shown in Fig. 7**e**, the rGO_0/C, $rGO_{1.25}$/C, $rGO_{2.5}$/C, $rGO_{5.0}$/C, and $rGO_{7.5}$/C samples all possessed negligible hemolysis ratio (<1%), indicating satisfying blood compatibility (see SI for the hemolysis calculation process). In addition, the inset of Fig. 7**e** displayed the visual appearance of the samples. Compared with the positive control, there was almost no red color in the supernatant of all the samples, further confirming the excellent blood compatibility of the PTL-coated magnetic Janus rGO/C microspheres. Moreover, we conducted coagulation assays by detecting the activated partial thromboplastin time (APTT) as well as

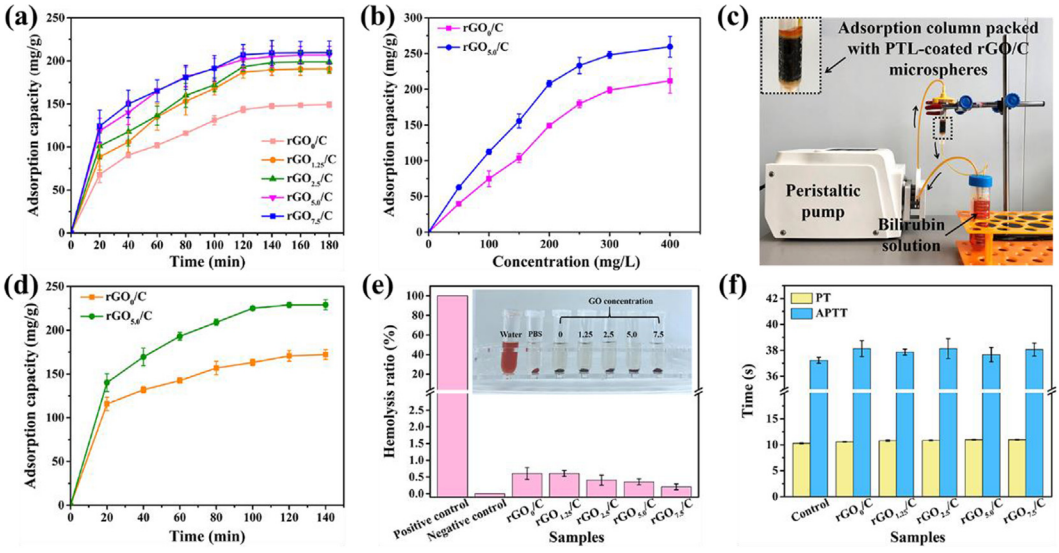

Fig. 7. (a) Plot of the adsorption dynamics of the PTL-coated magnetic Janus rGO/C microspheres with different rGO content for bilirubin uptake. The equilibrium uptake capacity of these samples was 149, 190, 198, 207, and 209 mg/g, respectively. (b) plots of the adsorption isotherms of the PTL-coated magnetic Janus rGO_0/C and $rGO_{5.0}$/C microspheres for bilirubin uptake; (c) digital photographs of the self-constructed simulated hemoperfusion device, the inserted picture is the adsorption column filled with the PTL-coated magnetic Janus rGO/C microspheres; (d) dynamic adsorption curves of PTL-coated magnetic Janus rGO_0/C and PTL-coated magnetic Janus $rGO_{5.0}$/C microspheres under simulated hemoperfusion process; (e) hemolysis ratio assays of the PTL-coated magnetic Janus rGO/C microspheres with distinct rGO content; (f) coagulation tests of the PTL-coated magnetic Janus rGO/C microspheres with distinct rGO content. All the tests were repeated 3 times.

prothrombin time (PT). For comparison, the rabbit blood plasma without adding microspheres was served as the control group. Specifically, the APTT values of rGO_0/C, $rGO_{1.25}$/C, $rGO_{2.5}$/C, $rGO_{5.0}$/C, and $rGO_{7.5}$/C microspheres were 38.13 s, 37.87 s, 38.13 s, 37.67 s, 38.06 s, respectively (Fig. 7**f**). In addition, the PT values of rGO_0/C, $rGO_{1.25}$/C, $rGO_{2.5}$/C, $rGO_{5.0}$/C, and $rGO_{7.5}$/C microspheres were 10.57 s, 10.8 s, 10.83 s, 10.97 s, 10.97 s, respectively (Fig. 7**g**). On the contrary, the APTT and PT value for the control group were 37.23 s and 10.3 s, lower than any of the experimental groups. It could be concluded that the PTL-coated magnetic Janus rGO/C microspheres exhibited slight anticoagulant performance. Taken together, the considerable blood compatibility and anticoagulant performance demonstrated the application value of the PTL-coated magnetic Janus rGO/C microspheres in blood purification.

3. Conclusion

On the basis of the previously reported preparative methods [21,31,32,41], we have successfully developed magnetic Janus rGO/C composite microspheres with integrated characteristics of size uniformity, controllable movement, and tailored surface wettability. First, a double-channel microfluidic device was employed to prepare the microspheres with uniform particle size. With that, the obtained microspheres were impatred with stable adsorption performance. Additionally, the magnetic Janus structure endowed the rGO/C composite microspheres with magnetic-responsive motion ability, thereby achieving precise manipulation of the microspheres. As a result, the recovery of the microspheres as well as the the collection of adsorbates could be achieved. Furthermore, by taking advantage of the magnetic Janus structure, the large-area of the microspheres could be coated with PTL nanofilm, which modified the coated area hydrophilic while un-coated area maintained hydrophobic, a feature similar to previous reported works [40,41]. Owing to such a combinational wettability feature, the magnetic Janus rGO/C composite microspheres allowed for versatile adsorption applications in different scenarios. On one hand, the bare, hydrophobic magnetic Janus rGO/C composite microspheres showed outstanding performance in cleaning organic solvents floating on top of the water. On the other hand, the PTL-coated magnetic Janus rGO/C composite microspheres displayed equally remarkable removal ability for pollutants underwater with a maximum adsorption capacitty of 35 g/g. More importantly, the PTL coated-magnetic Janus rGO/C composite microspheres owned satisfactory blood compatibility and exhibited extraordinarily high efficiency in both static adsorption and dynamic adsorption of bilirubin. Obviously, compared with previously similar carbon-based microparticles [18–20,37,50–52], our magnetic Janus rGO/C composite microspheres possess more broad practical functions, as listed in **Table S4**. Given these satisfying performance, we believe that the such magnetic Janus rGO/C composite microspheres are promising multifunctional adsorbents for both water purification and clinic hemoperfusion therapy. However, the features of the microspheres need to be further enriched, thus realizing pratical application in more complex scenarios. Meanwhile, we also hope that our work will provide a new perspective for fabrication of multifunctional microparticles.

CRediT authorship contribution statement

Xiaomin Ye: Formal analysis, Investigation, Writing – original draft. **Yunru Yu:** Formal analysis, Investigation. **Chaoyu Yang:** Formal analysis, Investigation. **Qihui Fan:** Writing – review & editing, Supervision, Funding acquisition. **Luoran Shang:** Conceptualization, Writing – review & editing, Supervision, Funding acquisition. **Fangfu Ye:** Conceptualization, Writing – review & editing, Supervision, Funding acquisition.

Declaration of Competing Interest

The authors declare that they have no known competing financial interests or personal relationships that could have appeared to influence the work reported in this paper.

Acknowledgments

This work was supported by the National Key Research and Development Program of China (2020YFA0908200), the National Natural Science Foundation of China (22002018), the Strategic Priority Research Program of Chinese Academy of Sciences (XDB33030300), the Youth Innovation Promotion Association of CAS (2021007), and the Program for Professor of Special Appointment (Eastern Scholar) at Shanghai Institutions of Higher Learning (SSH1340011).

Appendix A. Supplementary material

Supplementary data to this article can be found online at https://doi.org/10.1016/j.jcis.2022.05.156.

References

[1] Y. Kim, T. Kim, J. Lee, Y.S. Choi, J. Moon, S.Y. Park, T.H. Lee, M.-G. Lee, B.H. Hong, H.W. Jang, Tailored Graphene Micropatterns by Wafer-Scale Direct Transfer for Flexible Chemical Sensor Platform Adv, Mater. 33 (2020) 2004827.
[2] S.Y. Lim, H.W. Luan, S.W. Zhao, Y.J. Lee, Y.H. Zhang, Y.G. Huang, J.A. Rogers, J.H. Ahn, Assembly of Foldable 3D Microstructures Using Graphene Hinges, Adv. Mater. 32 (2020) 2001303.
[3] C. Zhang, S. Liang, W. Liu, F.T. Eickemeyer, X. Cai, K.e. Zhou, J. Bian, H. Zhu, C. Zhu, N. Wang, Z. Wang, J. Zhang, Y. Wang, J. Hu, H. Ma, C. Xin, S.M. Zakeeruddin, M. Grätzel, Y. Shi, Ti1–graphene single-atom material for improved energy level alignment in perovskite solar cells, Nat. Energy 6 (12) (2021) 1154–1163.
[4] I. Kaminska, J. Bohlen, R. Yaadav, P. Schüler, P. Tinnefeld, M. Raab, T. Schröder, J. Zähringer, K. Zielonka, S. Krause, P. Tinnefeld, Graphene Energy Transfer for Single-Molecule Biophysics, Biosensing, and Super-Resolution Microscopy, Adv. Mater. 33 (2021) 2101099.
[5] H.B. Huang, H.D. Shi, P. Das, J.Q. Qin, Y.G. Li, Z.-S. Wu, H.M. Cheng, The Chemistry and Promising Applications of Graphene and Porous Graphene Materials, Adv. Funct. 30 (Mater 2020,) 1909035.
[6] L. Han, H. Bi, X. Xie, S. Su, P. Mao, L. Sun, Superhydrophobic graphene-coated sponge with microcavities for high efficiency oil-in-water emulsion separation, Nanoscale 12 (34) (2020) 17812–17820.
[7] Y.R. Sun, F. Yu, L.Q. Li, J. Ma, Adsorption-Reduction Synergistic Effect for Rapid Removal of Cr (VI) ions on Superelastic NH2 -Graphene Sponge, Chem. Eng. J 421 (2021) 129933.
[8] H.T. Wang, X.Y. Mi, Y. Li, S.H. Zhan, 3D Graphene-Based Macrostructures for Water Treatment, Adv. Mater. 32 (2020) e1806843.
[9] C.H. Huang, Y.L. Zhao, Y.L. Li, Graphdiyne: The Fundamentals and Application of an Emerging Carbon Material, Adv. Mater. 31 (2019) e1904885.
[10] K.D. Patel, R.K. Singh, H.-W. Kim, Carbon-based nanomaterials as an emerging platform for theranostics, Mater. Horiz. 6 (3) (2019) 434–469.
[11] J.M. Kim, W. Jang, J.H. Kim, C.-M. Yang, Synthesis of graphene quantum dots-coated hierarchical CuO microspheres composite for use as binder-free anode for lithium-ion batteries, Compos. B. Eng. 222 (2021) 109083.
[12] S. Wang, Y.e. Niu, C. Wang, F. Wang, Z. Zhu, H. Sun, W. Liang, A.n. Li, Modified Hollow Glass Microspheres/Reduced Graphene Oxide Composite Aerogels with Low Thermal Conductivity for Highly Efficient Solar Steam Generation, ACS Appl. Mater. Interfaces 13 (36) (2021) 42803–42812.
[13] Y.H. Cui, K. Yang, J.Q. Wang, T. Shah, Q.Y. Zhang, B.L. Zhang, Preparation of pleated RGO/MXene/Fe3O4 microsphere and its absorption properties for electromagnetic wave, Carbon 172 (2021) 1–14.
[14] A. Raza, S.E. Alavi, F.B. Sime, F.Y. Han, J.A. Roberts, A. Popat, J.R. Falconer, T. Kumeria, Microfluidic assembly of pomegranate-like hierarchical microspheres for efflux regulation in oral drug delivery, Acta Biomater. 126 (2021) 277–290.
[15] X.D. Yang, Y.S. Wan, Y.L. Zheng, F. He, Z.B. Yu, J. Huang, H.L. Wang, Y.S. Ok, Y.S. Jiang, B. Gao, Surface functional groups of carbon-based adsorbents and their roles in the removal of heavy metals from aqueous solutions: A critical review, Chem Eng J 366 (2019) 608–621.
[16] A. Tyagi, Y.W. Ng, M. Tamtaji, I.H. Abidi, J. Li, F. Rehman, M.D. Hossain, Y. Cai, Z. Liu, P.R. Galligan, S. Luo, K. Zhang, Z. Luo, Elimination of Uremic Toxins by

Functionalized Graphene-Based Composite Beads for Direct Hemoperfusion, ACS Appl. Mater. Interfaces 13 (5) (2021) 5955–5965.
[17] S. Kong, Q. Zhang, L. Yang, Y. Huang, M. Liu, G. Yan, H. Zhao, M. Wu, X. Zhang, P. Yang, W. Cao, Effective Enrichment Strategy Using Boronic Acid-Functionalized Mesoporous Graphene-Silica Composites for Intact N- and O-Linked Glycopeptide Analysis in Human Serum, Anal. Chem. 93 (17) (2021) 6682–6691.
[18] Y. Cheng, Y. Cai, Z. Wang, X. Lu, H. Xia, Ultralight NiCo@rGO aerogel microspheres with magnetic response for oil/water separation, Chem. Eng. J. 430 (2022) 132894.
[19] Z. Luo, X. Wang, D. Yang, S. Zhang, T. Zhao, L. Qin, Z.-Z. Yu, Photothermal hierarchical carbon nanotube/reduced graphene oxide microspherical aerogels with radially orientated microchannels for efficient cleanup of crude oil spills, J. Colloid Interf. Sci. 570 (2020) 61–71.
[20] K. Wu, X. Liu, Z. Li, Y. Jiao, C. Zhou, Fabrication of chitosan/graphene oxide composite aerogel microspheres with high bilirubin removal performance, Mater. Sci. Eng. C 106 (2020) 110162.
[21] J. Chen, Y. Ma, L. Wang, W. Han, Y. Chai, T. Wang, J. Li, L. Ou, Preparation of chitosan/SiO_2-loaded graphene composite beads for efficient removal of bilirubin, Carbon 143 (2019) 352–361.
[22] G. Chen, Y. Yu, X. Wu, G. Wang, G. Gu, F. Wang, J. Ren, H. Zhang, Y. Zhao, Microfluidic Electrospray Niacin Metal-Organic Frameworks Encapsulated Microcapsules for Wound Healing, Research 2019 (2019) 1–11.
[23] C. Shao, Y. Liu, J. Chi, J. Wang, Z.e. Zhao, Y. Zhao, Responsive Inverse Opal Scaffolds with Biomimetic Enrichment Capability for Cell Culture, Research Article, Research 2019 (2019) 1–10.
[24] Y. Yu, J. Guo, L. Sun, X. Zhang, Y. Zhao, Microfluidic Generation of Microsprings with Ionic Liquid Encapsulation for Flexible Electronics, Research 2019 (2019) 1–9.
[25] Y. Han, J. Yang, W. Zhao, H. Wang, Y. Sun, Y. Chen, J. Luo, L. Deng, X. Xu, W. Cui, H. Zhang, Biomimetic injectable hydrogel microspheres with enhanced lubrication and controllable drug release for the treatment of osteoarthritis, Bioact. Mater. 6 (10) (2021) 3596–3607.
[26] L.J. Lei, Y.L. Zhu, X.Y. Qin, S.L. Chai, G.X. Liu, W.T. Su, Q.Z. Lv, D. Li, Magnetic biohybrid microspheres for protein purification and chronic wound healing in diabetic mice, Chem. Eng. J 425 (2021) 130671.
[27] J.Y. Shi, P. Zhu, S.F. Zhao, C. Xu, F.H. Yan, R.Q. Shen, H.M. Xia, H.Y. Jiang, S.Y. Xu, F.Q. Zhao, Continuous spheroidization strategy for explosives with micro/nano hierarchical structure by coupling microfluidics and spray drying, Chem. Eng. J 412 (2021) 128613.
[28] J. Yang, Y. Han, J. Lin, Y. Zhu, F. Wang, L. Deng, H. Zhang, X. Xu, W. Cui, Ball-Bearing-Inspired Polyampholyte-Modified Microspheres as Bio-Lubricants Attenuate Osteoarthritis, Small 16 (44) (2020) 2004519.
[29] T.T. Kong, H.C. Shum, D.A. Weitz, The Fourth Decade of Microfluidics, Small 16 (2020) 2000070.
[30] W.J. Liu, W. Bi, Y. Sun, L. Wang, X. Yu, R.Y. Cheng, Y.C. Yu, W.G. Cui, Biomimetic organic-inorganic hybrid hydrogel electrospinning periosteum for accelerating bone regeneration, Mater. Sci. Eng. 110 (2020) 110670.
[31] J.Y. Sim, G.H. Lee, S.-H. Kim, Microfluidic Design of Magnetoresponsive Photonic Microcylinders with Multicompartments, Small 11 (37) (2015) 4938–4945.
[32] L. Yang, Y. Liu, L. Sun, C. Zhao, G. Chen, Y. Zhao, Biomass Microcapsules with Stem Cell Encapsulation for Bone Repair Nano-Micro Lett. 14 (2022) 1–12.
[33] L. Yang, L. Sun, H. Zhang, F. Bian, Y. Zhao, Ice-Inspired Lubricated Drug Delivery Particles from Microfluidic Electrospray for Osteoarthritis Treatment, ACS Nano 15 (12) (2021) 20600–20606.
[34] R. Yu, Y. Shi, D. Yang, Y. Liu, J. Qu, Z.-Z. Yu, Graphene Oxide/Chitosan Aerogel Microspheres with Honeycomb-Cobweb and Radially Oriented Microchannel Structures for Broad-Spectrum and Rapid Adsorption of Water Contaminants, ACS Appl. Mater. Interfaces 9 (26) (2017) 21809–21819.
[35] A.n. Ouyang, Q. Gong, J.i. Liang, Carbon Nanotube-Chitosan Composite Beads with Radially Aligned Channels and Nanotube-Exposed Walls for Bilirubin Adsorption, Adv. Eng. Mater. 17 (4) (2015) 460–466.
[36] L.B. Yu, J. Liu, S.S. He, C.F. Huang, Z.L. Gong, L.H. Gan, M.N. Long, N-doped rGO/C@Si composites using sustainable chitosan as the carbon source for lithium-ion batteries, Appl. Surf. Sci. 501 (2020) 144136.
[37] W.S. Tan, R.J. Fu, H. Ji, Y. Kong, Y.G. Xu, Y. Qin, Preparation of nitrogen-doped carbon using graphene Quantum dots-chitosan as the precursor and its supercapacitive behaviors, Int. J. Biol. Macromol. 112 (2018) 561–566.
[38] Z.T. Li, X.H. Huang, K.K. Wu, Y.P. Jiao, C.R. Zhou, Fabrication of regular macro-mesoporous reduced graphene aerogel beads with ultra-high mechanical property for efficient bilirubin adsorption, Mater. Sci. Eng. C 106 (2020) 110282.
[39] X. Tong, Z.H. Chen, H. Zhuo, Y.J. Hu, S.S. Jing, J.C. Liu, L.X. Zhong, Tailoring the physicochemical properties of chitosan-derived N-doped carbon by controlling hydrothermal carbonization time for high-performance supercapacitor application, Carbohydr. Polym. 207 (2019) 764–774.
[40] W. Zhan, S. Yu, L. Gao, F. Wang, X. Fu, G. Sui, X. Yang, Bioinspired Assembly of Carbon Nanotube into Graphene Aerogel with "Cabbagelike" Hierarchical Porous Structure for Highly Efficient Organic Pollutants Cleanup, ACS Appl. Mater. Interfaces 10 (1) (2018) 1093–1103.
[41] X.M. Ye, C.M. Shao, Q.H. Fan, L.R. Shang, F.F. Ye, Porous carbon nanotube microspheres with tailorable surface wettability areas for oil adsorption, J. Colloid Interf. Sci. 604 (2021) 737–745.
[42] R.R. Liu, J. Zhao, Q. Han, X.Y. Hu, D. Wang, X. Zhang, P. Yang, One-Step Assembly of a Biomimetic Biopolymer Coating for Particle Surface Engineering, Adv. Mater. 30 (2018) e1802851.
[43] B. Saif, W.X. Zhang, X. Zhang, Q. Gu, P. Yang, Sn-Triggered Two-Dimensional Fast Protein Assembly with Emergent Functions, ACS Nano 13 (2019) 7737749.
[44] F. Yang, Z. Yan, J. Zhao, S. Miao, D. Wang, P. Yang, Rapid capture of trace precious metals by amyloid-like protein membrane with high adsorption capacity and selectivity, J. Mater. Chem. A 8 (6) (2020) 3438–3449.
[45] Y. Dhar, Y. Han, Current developments in biofilm treatments: Wound and implant infections, Engineered Regeneration 1 (2020) 64–75.
[46] Y. Chai, Z. Liu, Y. Du, L. Wang, J. Lu, Q. Zhang, W. Han, T. Wang, Y. Yu, L. Sun, L. Ou, Hydroxyapatite reinforced inorganic-organic hybrid nanocomposite as high-performance adsorbents for bilirubin removal in vitro and in pig models, Bioact. Mater. 6 (12) (2021) 4772–4785.
[47] M.F. Li, X.L. Wang, G.D. Gong, X. Li, Y. Tang, Q. Wang, J.B. Zhou, J.L. Guo, X.P. Liao, B. Shi, Engineered Liver-Inspired Collagen Matrix as a High-Performance Hemoperfusion Adsorbent for Bilirubin Removal, Chem. Eng. J 426 (2021) 130791.
[48] S. Kato, K.-I. Otake, H. Chen, I. Akpinar, C.T. Buru, T. Islamoglu, R.Q. Snurr, O.K. Farha, Zirconium-Based Metal-Organic Frameworks for the Removal of Protein-Bound Uremic Toxin from Human Serum Albumin, J. Am. Chem. Soc. 141 (6) (2019) 2568–2576.
[49] X. Song, X.H. Huang, Z.X. Li, Z.T. Li, K.J. Wu, Y.P. Jiao, C.R. Zhou, Construction of blood compatible chitin/graphene oxide composite aerogel beads for the adsorption of bilirubin, Carbohydr. Polym. 207 (2019) 704–712.
[50] R. Zhao, T.T. Ma, F.C. Cui, Y.Y. Tian, G.S. Zhu, Porous Aromatic Framework with Tailored Binding Sites and Pore Sizes as a High-Performance Hemoperfusion Adsorbent for Bilirubin Removal, Adv. Sci. 7 (2020) 2001899.
[51] L. Qiao, Y. Li, Y. Liu, Y. Wang, K. Du, High-strength, blood-compatible, and high-capacity bilirubin adsorbent based on cellulose-assisted high-quality dispersion of carbon nanotubes, J. Chromatogr. A 1634 (2020) 461659.
[52] M. Chen, H. Wu, Z. Li, K. Wu, Y. Jiao, C. Zhou, Preparation of reduced graphene oxide porous beads for lipase immobilization and its application for oil adsorption and glycerolysis reaction in situ, Micropor. Mesopor. Mat. 294 (2020) 109920.